Room-Temperature Detection of a Single Molecule's Absorption by Photothermal Contrast

A. Gaiduk, *et al.*

Science **330**, 353 (2010);
DOI: 10.1126/science.1195475

component block copolymer melts. The σ phase is the approximant crystal structure to certain dodecagonal quasicrystals, and an example of both σ-phase and quasicrystal formation has been reported in a single-dendrimer compound (*17*, *26*). Hayashida *et al*. also reported a dodecagonal quasicrystal in cylinder forming binary blends of star block terpolymer and homopolymer based on the nonperiodic tiling of TEM micrographs with $3^2.4.3.4$ nets (*25*). Molecular simulations indicate that dodecagonal quasicrystals represent slowly evolving metastable states relative to the (equilibrium) σ phase (*18*). Our time-dependent SAXS (Figs. 2 and 3) and mechanical spectroscopy (fig. S2) experiments with IL-15 may reflect a transient quasicrystalline morphology, consistent with these simulations. Appropriately designed block copolymers could represent ideal materials with which to characterize the thermodynamic and kinetic properties of these fascinating aperiodic systems.

Identification of the σ phase in linear block copolymer melts presents the opportunity for designing interesting and useful materials from many other polymers. Decades of experimental experience and well-established theory show that single-component block copolymer melts exhibit universal phase behavior, governed by well-established molecular parameters, primarily the molecular weight, composition, and segment-segment interaction parameter χ (*8*). The σ phase has an enormous unit cell, with lattice parameters that are expected to scale with the two-thirds power of block copolymer molecular weight. Thus, an asymmetric diblock copolymer prepared with 20 times the molecular weight of IL-15 (i.e., a modest 80 kg/mol), and subject to judicious choice of block types (which controls χ), should result in a unit cell dimension of $a \approx 0.3$ μm, potentially suitable for application as a photonic crystal (*35*). More generally, the concept of guiding the growth of gigantic crystals and quasicrystals by tailoring the packing frustration of soft macromolecules might be extended to other organic and inorganic nanoparticles by attaching polymer chains with controlled molecular weight and polydispersity to the surfaces.

References and Notes

1. J. Wittlinger, R. Fischer, S. Werner, J. Schneider, H. Schulz, *Acta Crystallogr. B* **53**, 745 (1997).
2. N. W. Ashcroft, N. D. Mermin, *Solid State Physics* (Brooks/Cole, Belmont, CA, 1976).
3. N. A. Clark, A. J. Hurd, B. J. Ackerson, *Nature* **281**, 57 (1979).
4. P. N. Pusey, W. van Megen, *Nature* **320**, 340 (1986).
5. L. Meng *et al*., *Nano Lett.* **6**, 2249 (2006).
6. J. M. Seddon, *Biochim. Biophys. Acta* **1031**, 1 (1990).
7. B. M. Rosen *et al*., *J. Am. Chem. Soc.* **131**, 17500 (2009).
8. F. S. Bates, G. H. Fredrickson, *Phys. Today* **52**, 32 (1999).
9. D. M. Anderson, S. M. Gruner, S. Leibler, *Proc. Natl. Acad. Sci. U.S.A.* **85**, 5364 (1988).
10. M. Matsen, F. S. Bates, *Macromolecules* **29**, 7641 (1996).
11. L. Leibler, *Macromolecules* **13**, 1602 (1980).
12. F. S. Bates, R. E. Cohen, C. V. Berney, *Macromolecules* **15**, 589 (1982).
13. S. Alexander, J. McTague, *Phys. Rev. Lett.* **41**, 702 (1978).
14. D. Levine, P. J. Steinhardt, *Phys. Rev. Lett.* **53**, 2477 (1984).
15. D. Shechtman, I. Blech, D. Gratias, J. W. Cahn, *Phys. Rev. Lett.* **53**, 1951 (1984).
16. C. Janot, *Quasicrystals: A Primer* (Oxford Univ. Press, New York, ed. 2, 1994).
17. X. Zeng *et al*., *Nature* **428**, 157 (2004).
18. A. S. Keys, S. C. Glotzer, *Phys. Rev. Lett.* **99**, 235503 (2007).
19. M. Dzugutov, *Phys. Rev. A* **46**, R2984 (1992).
20. J. Roth, A. R. Denton, *Phys. Rev. E Stat. Phys. Plasmas Fluids Relat. Interdiscip. Topics* **61**, (6 Pt B), 6845 (2000).
21. F. C. Frank, J. S. Kasper, *Acta Crystallogr.* **12**, 483 (1959).
22. G. Ungar, X. Zeng, *Soft Matter* **1**, 95 (2005).
23. R. Lifshitz, H. Diamant, *Philos. Mag.* **87**, 3021 (2007).
24. T. Dotera, *Philos. Mag.* **87**, 3011 (2007).
25. K. Hayashida, T. Dotera, A. Takano, Y. Matsushita, *Phys. Rev. Lett.* **98**, 195502 (2007).
26. G. Ungar, Y. Liu, X. Zeng, V. Percec, W. D. Cho, *Science* **299**, 1208 (2003).
27. S. C. Schmidt, M. A. Hillmyer, *Macromolecules* **32**, 4794 (1999).
28. M. J. Bluemle, J. Zhang, T. P. Lodge, F. S. Bates, *Macromolecules* **43**, 4449 (2010).
29. M. B. Kossuth, D. C. Morse, F. S. Bates, *J. Rheol.* **43**, 167 (1999).
30. The integrity of sample SISO-3 after 24 hours of annealing under vacuum at 140°C was verified by size exclusion chromatography (SEC).
31. A. C. Lawson *et al*., *Acta Crystallogr. B* **44**, 89 (1988).
32. A. Arakcheeva, G. Chapuis, H. Birkedal, P. Pattison, V. Grinevitch, *Acta Crystallogr. B* **59**, 324 (2003).
33. G. J. Dickins, A. M. B. Douglas, W. H. Taylor, *Acta Crystallogr.* **9**, 297 (1956).
34. J. W. Elmer, T. A. Palmer, E. D. Specht, *Metall. Mater. Trans., A Phys. Metall. Mater. Sci.* **38**, 464 (2007).
35. J. D. Joannopoulos, S. G. Johnson, J. N. Winn, R. D. Meade, *Photonic Crystals: Molding the Flow of Light* (Princeton Univ. Press, Princeton, NJ, ed. 2, 2008).

36. This work was supported by the Department of Energy through a subcontract to UT-Battelle (4000041622), the National Science Foundation through grant DMR-0704192, and the University of Minnesota Materials Research Science and Engineering Center (MRSEC). Portions of this work were performed at the DuPont-Northwestern-Dow Collaborative Access Team (DND-CAT) located at Sector 5 of the Advanced Photon Source (APS). DND-CAT is supported by E. I. Dupont de Nemours & Company, the Dow Chemical Company, and the State of Illinois. Use of the APS was supported by the U.S. Department of Energy, Office of Science, Basic Energy Sciences, under contract DE-AC02-06CH11357. Parts of this work were carried out in the University of Minnesota I.T. Characterization Facility, which receives partial support from NSF through the National Nanotechnology Infrastructure Network program. The authors gratefully acknowledge helpful discussions with N. Balsara and T. P. Lodge.

Supporting Online Material

www.sciencemag.org/cgi/content/full/330/6002/349/DC1
Figs. S1 to S7
References

23 July 2010; accepted 3 September 2010
10.1126/science.1195552

Room-Temperature Detection of a Single Molecule's Absorption by Photothermal Contrast

A. Gaiduk, M. Yorulmaz, P. V. Ruijgrok, M. Orrit*

So far, single-molecule imaging has predominantly relied on fluorescence detection. We imaged single nonfluorescent azo dye molecules in room-temperature glycerol by the refractive effect of the heat that they release in their environment upon intense illumination. This photothermal technique provides contrast for the absorbing objects only, irrespective of scattering by defects or roughness, with a signal-to-noise ratio of ~10 for a single molecule in an integration time of 300 milliseconds. In the absence of oxygen, virtually no bleaching event was observed, even after more than 10 minutes of illumination. In a solution saturated with oxygen, the average bleaching time was of the order of 1 minute. No blinking was observed in the absorption signal. On the basis of bleaching steps, we obtained an average absorption cross section of 4 angstroms^2 for a single chromophore.

Single-molecule optical detection (*1*) has become an indispensable tool in molecular biology and materials science. For the past 20 years, optical single-molecule detection has relied on fluorescence (*2*, *3*) because of the low background of this technique. However, monitoring optical absorption more directly would have definite advantages. Fluorescence requires an efficient pathway for populating the emitting state and also the near absence of nonradiative relaxation to the ground state or to intermediate dark states. The fluorescent state is easily destroyed or quenched by photochemical reactions, often involving electron or proton transfer. Indeed, only a very small fraction of all absorbing molecules (called chromophores) are strongly fluorescent (then called fluorophores). Nonfluorescent chromophores include certain metal complexes and many conjugated molecules, for example, DNA bases, that are important in biology. Such molecules could become more-natural labels than fluorophores.

The first single-molecule optical detection experiment, by Kador and Moerner, was achieved by absorption (*4*) but relied on favorable cryogenic conditions, under which the absorption cross section of the narrowest molecular transition was extremely large. Their doubly modulated absorption technique was later improved on with modern optics and detectors (*5*–*7*), but the

Institute of Physics, Leiden University, Post Office Box 9504, 2300 RA Leiden, Netherlands.

*To whom correspondence should be addressed. E-mail: orrit@molphys.leidenuniv.nl

absorption signal still appears on a strong background of unabsorbed photons, resulting in a lower signal-to-noise ratio than fluorescence. Detecting the absorption of a single molecule at ambient conditions is much more challenging than at low temperature because of the reduction by 5 to 6 orders of magnitude of the cross section, essentially because of fast dephasing by thermal fluctuations. A method for the detection of single-molecule absorption at room temperature must thus solve two different problems.

First, the absorption cross section of a typical chromophore at room temperature is only of the order of 10^{-2} nm^2. The number of the absorption events varies as the ratio of the absorption cross section to the area of a diffraction-limited light beam. This ratio is about 10^{-7} for a laser spot diameter of 300 nm. Because statistical fluctuations in a number N of photons scale as $\sqrt{N}$, a change in transmitted signal of 10^{-7} requires more than 10^{14} photons to be detected. Of those, at least 10^7 have to be absorbed by the molecule. The detection of such small signals therefore requires many absorption events, which may conflict with the poor photostability of many fluorescent molecules at ambient conditions.

Second, in a direct extinction measurement, where only missing photons are identified, a molecule's absorption appears on a background of scattering by any inhomogeneities in refractive index, arising for instance from roughness of the interfaces. Therefore, for practical applications, it is vital to be able to discriminate true absorption from scattering.

Three main routes have been pursued in the past 10 years toward surmounting these obstacles.

Photothermal contrast relies on the intensity change of a probe beam caused by a modulated heating beam of a different color. Kitamori and co-workers (*8*) have detected sub-yoctomole concentrations of absorbers in solution with integration times of several seconds, that is, in conditions under which many diffusing molecules contributed in turn to the signal. Boyer *et al.* (*9*) applied a similar method to detect single immobilized gold nanoparticles down to 5 nm in diameter, a performance that was later substantially improved by Berciaud *et al.* (*10*, *11*) and has led to a number of applications in recent years.

Alternatively, various sensitive optical techniques have been applied either in interferometers (*12*) or in a reflection or transmission geometry (*13*, *14*) to detect some tens of molecules (*12*), small particles (*13*), or quantum dots (*15*). In the latter two cases, however, the use of ultraclean and stable conditions was essential to ensure the absence of scattering background.

Most recently, Xie and co-workers have explored stimulated emission to distinguish absorption from scattering (*16*). Indeed, because stimulated photons can only arise from the excited state of molecules, this method efficiently rejects scattering and fulfills the second requirement. With a modulated stimulating beam, they were able to image absorption in cells down to a few tens of molecules.

We pushed the sensitivity of photothermal detection to the single-molecule limit, demonstrating a signal-to-noise ratio of about 10 with reasonable integration times of 100 to 300 ms, joined to excellent rejection of the scattering background.

Photothermal contrast relies on a time-dependent thermal lens. This inhomogeneous refractive index profile results from the heat dissipated by a pointlike absorber in its surroundings. The local inhomogeneity of the refractive index scatters a probe beam. The resulting weak scattered field interferes with the main probe field (either transmitted or reflected), thereby slightly changing the detected probe intensity. A disadvantage of the method is that the transduction efficiency, relating the index change to the dissipated heat, is rather low. It is proportional to $\partial n/\partial T$, of the order of 10^{-4} K^{-1} or lower. However, this inefficiency is more than compensated for by a gain in applicable probe intensity and the associated reduction in photon noise. Because the probe wavelength can be chosen in a transparency region, a spectral range where absorption is negligible, the probe intensity can be very high, much higher than the saturation intensity of the heating beam. Photon noise on the probe beam is therefore considerably reduced.

Our setup for photothermal contrast imaging is shown in fig. S1 (*17*). The absorbed pump power gives rise to a temperature gradient with an amplitude $\Delta T_{surf} = \frac{\sigma_{abs} I_{heat}}{4\pi\kappa R}$ at the surface of the source, assumed to be spherical: σ_{abs} is the absorption cross section of the absorber, I_{heat} the pump intensity, κ the thermal conductivity of the medium, and R the radius of the heat source. The backward scattered probe light is collected by the focusing microscope objective, sent to a fast photodiode, and fed into the lock-in amplifier. The photothermal signal is proportional to both the heating and probe powers. We modulate the pump at rather high frequency (around 1 MHz) to reject mechanical, electronic, and laser noise. We have chosen the reflection geometry with index matching to adapt the probe signal to the characteristics of our fast low-noise detector (maximum detected intensity 18 μW). Because a good overlap of the two tightly focused beams with different colors is critical, residual chromatic aberrations of the objective must be carefully compensated.

We very recently used this setup (*18*) to improve the photothermal detection approach of

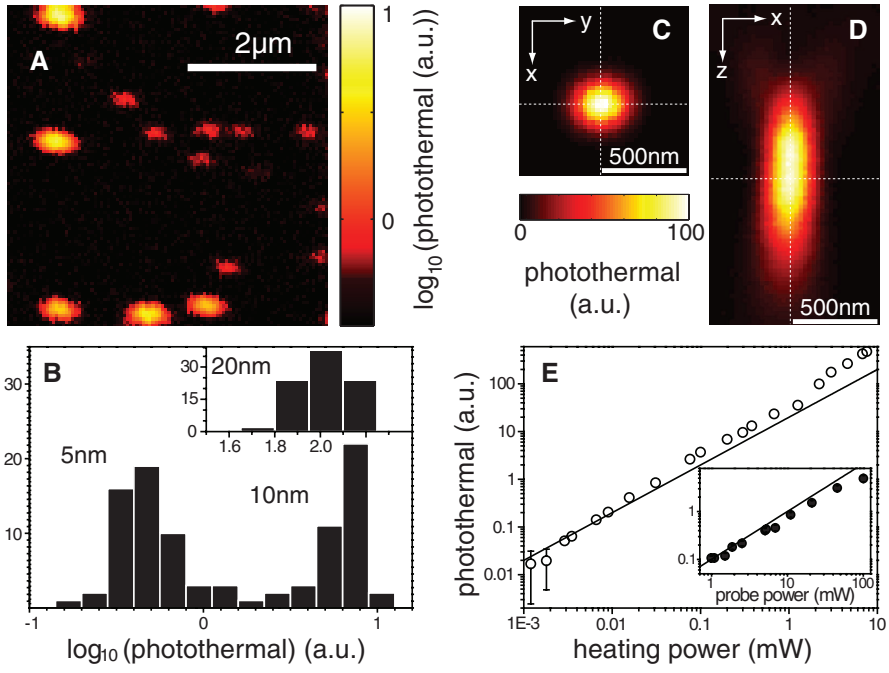

Fig. 1. Photothermal images of gold nanospheres illustrate the large dynamic range of the method and its low background. (**A**) A raster scan image of a sample containing 10-nm (yellow) and 5-nm (red) diameter gold particles in glycerol: heating power is 0.43 mW; probe power, 21 mW; integration time per pixel, 3 ms. The FWHMs of the photothermal spots are 210 nm and 370 nm. a.u., arbitrary units. (**B**) Histogram of the photothermal signals for 94 gold particles of 5-nm or 10-nm diameter. (Inset) Histogram of signals for 88 gold particles of 20-nm diameter in the same conditions. As expected, the photothermal signal roughly scales as the volume of the particles. (**C** and **D**) The point-spread function (PSF) of the photothermal signal is well fitted by a Gaussian with σ_x = 220 nm, σ_y = 250 nm, and σ_z = 670 nm, as mapped by scanning a 20-nm-diameter gold particle in three dimensions. Note the two weak lobes of the PSF in the *x*, *z* image, also observed in confocal fluorescence microscopy. These data are reproduced from (*18*). (**E**) Linear scaling of the photothermal signal of a 20-nm gold particle with heating and probe (inset) powers. Solid lines show linear fits at low heating and probe powers. Error bars indicate standard deviation values. For most of the data, they are smaller than the symbol size.

Berciaud *et al.* (*10*, *11*). Among the different points discussed in (*18*), the choice of the transducing fluid is crucial to enhance the sensitivity. We first characterized the sensitivity of our setup with gold nanoparticles used as absorption standards. Figure 1A shows an image of a sample containing 10-nm- and 5-nm-diameter gold spheres on glass surface in glycerol. We measured photothermal signals by heating at 514 nm and probing at 800 nm. The signals from different diameters differ by a factor of about 8, as expected from the volume ratio. The elongated shape of the photothermal spots in this image (210 nm and 370 nm principal half-maximum widths) arose from the shape of the pump beam, because spatial filtering was weak in this experiment. Stronger spatial filtering yielded a much better shape. In our previous work (*18*), we measured the photothermal detection volume by scanning a 20-nm gold sphere in three dimensions. The full widths at half maximum (FWHM, determined by a Gaussian fit) across *x*, *y*, and *z* are 220 nm, 250 nm, and 670 nm, respectively. These data are reproduced in Fig. 1, C and D. Last, we verified the linear relationships between pump and probe powers and photothermal signal by varying the heating power over 4 orders of magnitude (1 μW to 10 mW) and the probe power over 2 orders of magnitude (1 mW to 100 mW). Slight deviations from linear behavior at high power may be due to variations of spectra or thermal constants of the materials in the broad range of temperature changes explored (from 0.05 K up to about 500 K). Compared with our prior report (*18*), we exploit the thermal sensitivity of glycerol here but not the thermal isolation from the glass substrate.

To ascertain the possibility of detecting a single organic molecule in photothermal microscopy, we only need to compare the smallest detectable power over a given integration time to the power dissipated by a single molecule. In (*18*), we demonstrated the detection of a dissipated power as low as 3 nW with a signal-to-noise ratio of $SNR = 8$ and an integration time of 10 ms. By increasing the integration time to hundreds of ms, even smaller dissipated powers can be measured. A single molecule can release heat along two pathways: a direct nonradiative transition from the excited state and vibronic relaxation before and after a radiative fluorescent transition. The shorter the fluorescence lifetime (τ_F) and the lower the fluorescence quantum yield (η_F) are, the larger is the dissipated power at saturation. The most favorable molecules for photothermal detection should therefore have strong nonradiative channels and thus very weak fluorescence yields. This is the case for the trial molecules chosen in the present work. We calculated the dissipated power at saturation for several commercially available organic molecules (fig. S2 and table S1) (*17*). The highest dissipated power at saturation of 15 nW well above the limit of 3 nW was obtained for a high-efficiency dark quencher (Black-Hole-Quencher, BHQ1, Biosearch Technologies, Novato, California). This azo dye molecule is used in the design of oligonucleotide probes to quench the fluorescence of a dye in a DNA construct (*19*, *20*). For the present experiments, we chose a chromophore-DNA construct to increase the absorption signal by the presence of two chromophores in each construct and to secure the adhesion of the constructs to the glass surface by their single-strand DNA linker (figs. S3 and S4) (*17*).

A photothermal image obtained on a sample of spin-coated quencher-DNA construct (BHQ1-10T-BHQ1) submerged in nitrogen-bubbled glycerol is shown in Fig. 2A. The image reveals four photothermal spots with a $SNR \sim 10$ for an integration time of 300 ms. These spots persisted for as long as 1 hour without bleaching or fading. Less than 2% of the molecules bleached in the first 10 min of illumination. When the glycerol was saturated by oxygen, in contrast, one-step photobleaching was observed after an average time of ~1 min. Several typical background-corrected photothermal traces are displayed in Fig. 2B and demonstrate digital irreversible steps. We never observed any blinking or any later reappearance of a bleached photothermal signal.

The absolute value of the change in absorption cross section upon photobleaching is estimated by comparison to the photothermal signal of 20-nm gold nanoparticles. The calculated (*21*, *22*) cross section of these gold nanospheres is 460 nm^2 at 514 nm in glycerol, in good agreement with absolute cross-section measurements (*23*). The histogram in Fig. 2C summarizes the absorption cross-section changes in 30 single bleaching steps, with an average value of 4.1 $Å^2$. This value, which corresponds to the cross section of a single chromophore, is in satisfactory agreement with the isotropic value, $\sigma_{BHQ} = 2.1$ $Å^2$, deduced from the absorption spectrum of the quencher-DNA construct in glycerol. Note that the maximum value of the cross section for a favorably oriented molecule is $3\sigma_{BHQ} = 6.3$ $Å^2$. The histogram of Fig. 2C is a broad distribution without distinct maximum, in qualitative agreement with the isotropic distribution of transition dipole moments (solid line in Fig. 2C with a steplike cutoff at $3\sigma_{BHQ}$). Our observation suggests that the absorption dipoles of BHQ1 molecules are not freely rotating, even under the heavy illumination to which we subjected them, and that the molecules are fixed to the surface and/or to the DNA linker.

The histogram of survival times before digital photobleaching is shown in Fig. 2D. The average number of absorbed photons before bleaching is about 10^{11} under oxygen-saturated conditions and larger than 10^{12} under oxygen-free conditions, showing a huge reduction in the bleaching efficiency per photon compared with usual fluorophores in the same conditions. This robustness can be attributed to the much shorter dwell time in the excited singlet state resulting from the efficient internal conversion. We have attempted measurements of the polarization dependence of single-molecule absorption signals, but these

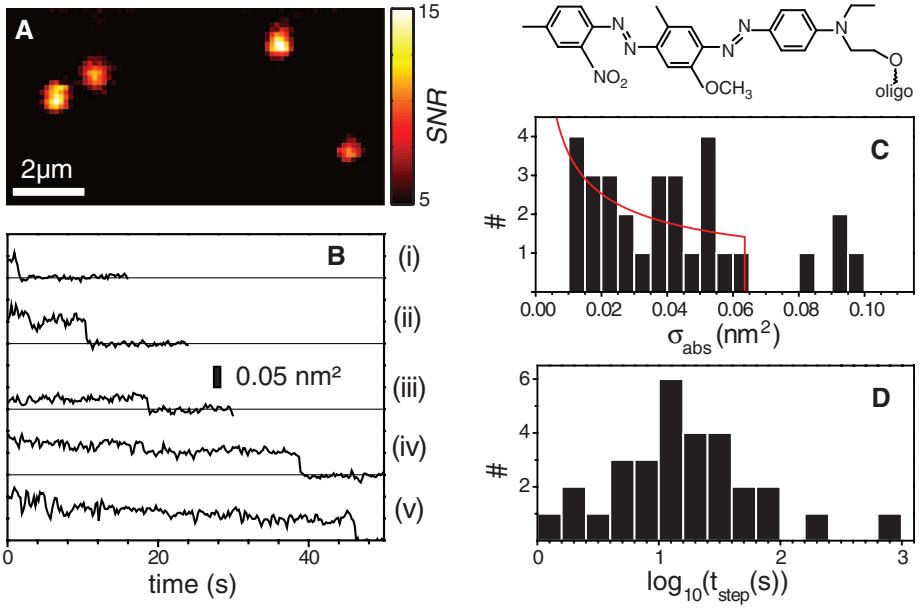

Fig. 2. (**A**) Photothermal image of four constructs (BHQ1-10T-BHQ1), consisting of two fluorescence quenchers (BHQ1) attached to a single strand of DNA (10 thymine bases): integration time per pixel, 300 ms; heating power, 5.1 mW at 514 nm; probe power, 84 mW at 800 nm. (**B**) Photothermal time traces showing single-step bleaching obtained on a sample with BHQ1-10T-BHQ1 on glass in oxygen-saturated glycerol: integration time per point, 100 ms; heating, 5.1 mW; probe, 84 mW. (**C**) Histogram of amplitude of 30 bleaching steps in the photothermal traces. The average change in absorption cross section upon bleaching is 4.1 $Å^2$. The red line represents the distribution of absorption cross sections of single chromophores corresponding to the isotropic distribution of transition dipole moments. The cutoff at 6.3 $Å^2$ is the calculated cross section for a perfectly oriented molecule. (**D**) Histogram of survival times before one-step photobleaching events for the same set of data. The average time is 49 s.

measurements were very difficult because of the buildup of a photothermal background over long illumination times by the pump beam [the probe had no noticeable effect on this buildup (figs. S6 to S8) (*17*)].

We could not observe simultaneous fluorescence and photothermal signals from the spots of Fig. 2. Such simultaneous signals arose only from abnormally bright spots, attributable to large aggregates, and showed quick correlated decays of both signals upon illumination (fig. S9) (*17*). On the sample of Fig. 2, we also observed a few spots with strong photothermal signals corresponding to an absorption cross section of about 1 nm^2, which shows one-step bleaching. Possible interpretations are aggregates of several molecules desorbing simultaneously or, more probably, another chemical species with a large absorption cross section, possibly with excited-state absorption of the intense probe beam. We only found very few examples of two-step photobleaching of the BHQ1-10T-BHQ1 constructs. We believe that this absence results from the low probability of bleaching, joined with the low probability of finding two favorable orientations in the same construct.

Our successful single molecule detection relied here on favorable conditions, the use of glycerol (with large $\partial n/\partial T$ and poor heat conduction) instead of water, with a high heating power of 5.1 mW focused into the diffraction-limited spot and with an even higher probe power of more than 70 mW. Although the conditions for single-molecule absorption in a cell, for example, would be far from these ideal ones, this result opens the way for further optimization of the technique and to a much broader variety of absorbing molecules. Interesting candidates are natural absorbers, for example, metal proteins such as hemoglobin, which would be useful for applications in analytical biochemistry and medical assays (*24*).

An intrinsic limitation of the photothermal method is the low transduction factor between pump and probe because of the relatively weak variation of refractive index with temperature. A future search for more-efficient transduction, for example, photomechanical or photoelectrical detections using micro- and nano-optomechanical systems (*25*), appears full of promise.

References and Notes

1. W. E. Moerner, M. Orrit, *Science* **283**, 1670 (1999).
2. M. Orrit, J. Bernard, *Phys. Rev. Lett.* **65**, 2716 (1990).
3. R. A. Keller *et al.*, *Appl. Spectrosc.* **50**, 12A (1996).
4. W. E. Moerner, L. Kador, *Phys. Rev. Lett.* **62**, 2535 (1989).
5. L. Kador, T. Latychevskaia, A. Renn, U. P. Wild, *J. Chem. Phys.* **111**, 8755 (1999).
6. J. Y. P. Butter, B. Hecht, B. R. Crenshaw, C. Weder, *J. Chem. Phys.* **125**, 154710 (2006).
7. I. Gerhardt *et al.*, *Phys. Rev. Lett.* **98**, 033601 (2007).
8. M. Tokeshi, M. Uchida, A. Hibara, T. Sawada, T. Kitamori, *Anal. Chem.* **73**, 2112 (2001).
9. D. Boyer, P. Tamarat, A. Maali, B. Lounis, M. Orrit, *Science* **297**, 1160 (2002).
10. S. Berciaud, L. Cognet, G. A. Blab, B. Lounis, *Phys. Rev. Lett.* **93**, 257402 (2004).
11. S. Berciaud, D. Lasne, G. A. Blab, L. Cognet, B. Lounis, *Phys. Rev. B* **73**, 045424 (2006).
12. J. Hwang, M. M. Fejer, W. E. Moerner, *Phys. Rev. A* **73**, 021802 (2006).
13. F. V. Ignatovich, L. Novotny, *Phys. Rev. Lett.* **96**, 013901 (2006).
14. G. Wrigge, J. Hwang, I. Gerhardt, G. Zumofen, V. Sandoghdar, *Opt. Express* **16**, 17358 (2008).
15. P. Kukura, M. Celebrano, A. Renn, V. Sandoghdar, *Nano Lett.* **9**, 926 (2009).
16. W. Min *et al.*, *Nature* **461**, 1105 (2009).
17. Materials and methods are available as supporting material on *Science* Online.
18. A. Gaiduk, P. V. Ruijgrok, M. Yorulmaz, M. Orrit, *Chem. Sci.* **1**, 343 (2010).
19. V. V. Didenko, Ed., *Methods in Molecular Biology: Fluorescent Energy Transfer Nucleic Acid Probes: Designs and Protocols* (Humana, Totowa, NJ, 2006).
20. S. A. E. Marras, F. R. Kramer, S. Tyagi, *Nucleic Acids Res.* **30**, e122 (2002).
21. M. A. van Dijk *et al.*, *Phys. Chem. Chem. Phys.* **8**, 3486 (2007).
22. C. F. Bohren, D. R. Huffman, *Absorption and Scattering of Light by Small Particles* (Wiley, New York, 1998).
23. A. Arbouet *et al.*, *Phys. Rev. Lett.* **93**, 127401 (2004).
24. S. Lu, W. Min, S. Chong, G. R. Holtom, X. S. Xie, *Appl. Phys. Lett.* **96**, 113701 (2010).
25. S. W. Stahl, E. M. Puchner, H. E. Gaub, *Rev. Sci. Instrum.* **80**, 073702 (2009).

26. We acknowledge financial support by European Research Council (Advanced Grant SiMoSoMa). This work is a part of the research program of the Stichting voor Fundamenteel Onderzoek der Materie, which is financially supported by the Netherlands Organization for Scientific Research. We thank H. van der Meer for precious help with the experimental setup.

Supporting Online Material

www.sciencemag.org/cgi/content/full/330/6002/353/DC1
Materials and Methods
Figs. S1 to S9
References

22 July 2010; accepted 16 September 2010
10.1126/science.1195475

Atmospheric CO_2: Principal Control Knob Governing Earth's Temperature

Andrew A. Lacis,* Gavin A. Schmidt, David Rind, Reto A. Ruedy

Ample physical evidence shows that carbon dioxide (CO_2) is the single most important climate-relevant greenhouse gas in Earth's atmosphere. This is because CO_2, like ozone, N_2O, CH_4, and chlorofluorocarbons, does not condense and precipitate from the atmosphere at current climate temperatures, whereas water vapor can and does. Noncondensing greenhouse gases, which account for 25% of the total terrestrial greenhouse effect, thus serve to provide the stable temperature structure that sustains the current levels of atmospheric water vapor and clouds via feedback processes that account for the remaining 75% of the greenhouse effect. Without the radiative forcing supplied by CO_2 and the other noncondensing greenhouse gases, the terrestrial greenhouse would collapse, plunging the global climate into an icebound Earth state.

It often is stated that water vapor is the chief greenhouse gas (GHG) in the atmosphere. For example, it has been asserted that "about 98% of the natural greenhouse effect is due to water vapour and stratiform clouds with CO_2 contributing less than 2%" (*1*). If true, this would imply that changes in atmospheric CO_2 are not important influences on the natural greenhouse capacity of Earth, and that the continuing increase in CO_2 due to human activity is therefore not relevant to climate change. This misunderstanding is resolved through simple examination of the terrestrial greenhouse.

The difference between the nominal global mean surface temperature (T_S = 288 K) and the global mean effective temperature (T_E = 255 K) is a common measure of the terrestrial greenhouse effect ($G_T = T_S - T_E$ = 33 K). Assuming global energy balance, T_E is also the Planck radiation equivalent of the 240 W/m^2 of global mean solar radiation absorbed by Earth.

The Sun is the source of energy that heats Earth. Besides direct solar heating of the ground, there is also indirect longwave (LW) warming arising from the thermal radiation that is emitted by the ground, then absorbed locally within the atmosphere, from which it is re-emitted in both upward and downward directions, further heating the ground and maintaining the temperature gradient in the atmosphere. This radiative interaction is the greenhouse effect, which was first discovered by Joseph Fourier in 1824 (*2*), experimentally verified by John Tyndall in 1863 (*3*), and quantified by Svante Arrhenius in 1896 (*4*). These studies established long ago that water vapor and CO_2 are indeed the principal terrestrial GHGs. Now, further consideration shows that CO_2 is the one that controls climate change.

CO_2 is a well-mixed gas that does not condense or precipitate from the atmosphere. Water vapor and clouds, on the other hand, are highly active components of the climate system that respond rapidly to changes in temperature and air pressure by evaporating, condensing, and precipitating. This identifies water vapor and clouds as the fast feedback processes in the climate system.

Radiative forcing experiments assuming doubled CO_2 and a 2% increase in solar irradiance (*5*) show that water vapor provides the strongest climate feedback of any of the atmospheric GHGs, but that it is not the cause (forcing) of global cli-

NASA Goddard Institute for Space Studies, 2880 Broadway, New York, NY 10025, USA.

*To whom correspondence should be addressed. E-mail: andrew.a.lacis@nasa.gov